nature geoscience

ARTICLES

PUBLISHED ONLINE: 28 MARCH 2016 | DOI: 10.1038/NGEO2686

Rockfall triggering by cyclic thermal stressing of exfoliation fractures

Brian D. Collins[1*] and Greg M. Stock[2]

Exfoliation of rock deteriorates cliffs through the formation and subsequent opening of fractures, which in turn can lead to potentially hazardous rockfalls. Although a number of mechanisms are known to trigger rockfalls, many rockfalls occur during periods when likely triggers such as precipitation, seismic activity and freezing conditions are absent. It has been suggested that these enigmatic rockfalls may occur due to solar heating of rock surfaces, which can cause outward expansion. Here we use data from 3.5 years of field monitoring of an exfoliating granite cliff in Yosemite National Park in California, USA, to assess the magnitude and temporal pattern of thermally induced rock deformation. From a thermodynamic analysis, we find that daily, seasonal and annual temperature variations are sufficient to drive cyclic and cumulative opening of fractures. Application of fracture theory suggests that these changes can lead to further fracture propagation and the consequent detachment of rock. Our data indicate that the warmest times of the day and year are particularly conducive to triggering rockfalls, and that cyclic thermal forcing may enhance the efficacy of other, more typical rockfall triggers.

Rockfalls are common and hazardous in steep terrains around the world[1–4], and are primary agents of landscape erosion in many environments[4–8]. In exfoliating landscapes (Fig. 1a), rockfalls frequently occur as detachments of the outer rock layers (exfoliation sheets) along surface-parallel fractures (joints). These detachments are typically thinner (measured normal to rock faces) than they are wide or long. The origin and formation of exfoliation sheets, particularly those formed in granitic landscapes, has been a subject of interest for more than a century[9–15]. The consensus that erosion-induced or palaeo-stresses are responsible for their formation has been challenged by recent work[16,17] proposing that a combination of regional compressive stresses and topographic curvature can generate exfoliation fractures. Regardless of their origin, understanding modern-day failure of rock masses along exfoliation fractures is important for studies of landscape erosion and rockfall hazards.

Rockfalls can be triggered by a number of mechanisms, including precipitation, seismic shaking, and freeze–thaw conditions[6,18]. Yet many rockfalls lack recognized triggers and are seemingly spontaneous events, suggesting other factors at play. The role of thermal effects (temperature and insolation) on initiating rock deformation, where rock surfaces expand, contract, and eventually fail in response to cyclical temperature variations, was critically examined regarding exfoliation sheet formation, and subsequently dismissed[11,19,20]. However, these studies did not investigate what role thermal effects might have on the deformation of existing exfoliation sheets. Further, some studies[13] acknowledged that thermal effects could be important at depths of less than one metre—areas of obvious interest for rockfalls. Recent studies on building façade construction show that anisotropic and differential expansion of rock-forming minerals can cause thermally driven deformation in a range of rock types when cyclical temperature fluctuations are applied to thin sheet-like structures[21–23]. In addition, studies of differential weathering of boulders in arid environments[24–26] indicate that insolation-induced radial thermal gradients may generate tensile stresses in decimetre- to metre-scale boulders. Other work verifies that some form of cyclic thermally induced deformation occurs in unstable rock masses, whether by long-term creep of detached blocks or by short-term fracture propagation in competent rock[27–30]. In only one previous study[31] has the role of thermal stress in exfoliation sheets been related to how this might trigger rockfalls.

Here we present new empirical and quantitative evidence linking rockfalls with thermal–mechanical forcing of exfoliation fractures. Using 3.5 years of temperature, light intensity, humidity and crack aperture data measured on a near-vertical, 19-m-tall, 4-m-wide, 10-cm-thick granodiorite exfoliation sheet in Yosemite Valley, California, USA (Fig. 1), we show how cyclic thermal forcing can progressively fracture exfoliation sheets and trigger rockfalls. Yosemite Valley is located in the central Sierra Nevada—a mountain range well known for an abundance of exfoliation features[9,10]. Our explanation of exfoliation sheet deformation and detachment uniquely incorporates a broad range of scientific and engineering principles, including thermodynamics, structural beam theory, and fracture mechanics. These concepts are applicable to other exfoliating environments worldwide.

Cyclic and cumulative deformation measurements

Crack aperture data measured with specially designed 'crackmeters' installed behind the partially detached exfoliation sheet (Fig. 1b; see Methods), along with differential terrestrial lidar topographic surveying results (Fig. 1c), reveal an asymmetrically subarcuate deformation pattern with maximum daily opening at the midpoint of the sheet, slightly less opening towards the bottom, and the least opening near the top. The data indicate both diurnal and seasonal cyclical deformation trends with strong temporal temperature coupling (Fig. 2). Outward deformation at the midpoint of the sheet averages 8 mm d^{-1}, with a maximum of 13 mm d^{-1}. Maximum outward deformation occurs in the afternoon (approximately 13:00 to 16:00) when temperatures are highest; maximum inward deformation occurs in the mid-morning (approximately 7:00 to 9:00) when temperatures are still low. Deformation also generally tracks the light intensity response, with expansion during peak

[1]US Geological Survey, Landslide Hazards Program, 345 Middlefield Road, MS-973, Menlo Park, California 94025, USA. [2]National Park Service, Yosemite National Park, El Portal, California 95318, USA. *e-mail: bcollins@usgs.gov

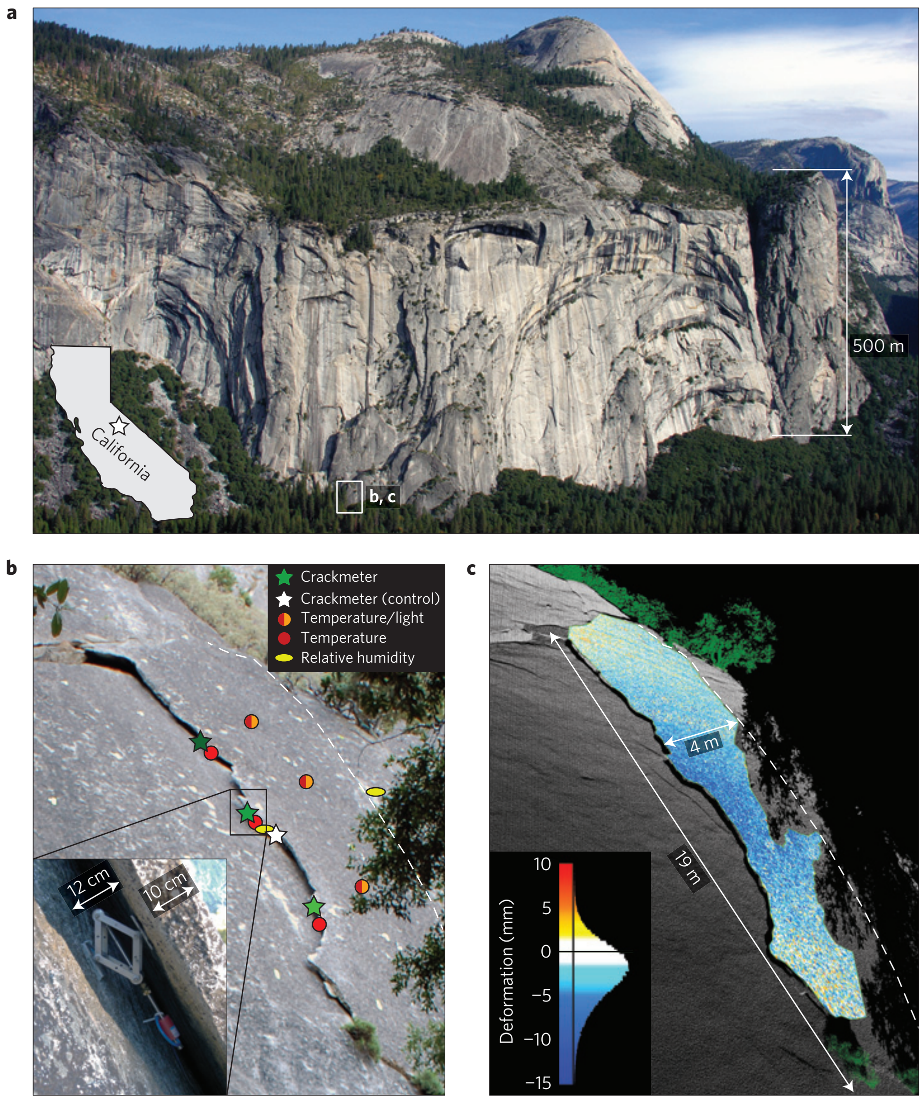

Figure 1 | Rockfall-prone cliffs and monitored exfoliation sheet in Yosemite Valley. a, Yosemite exhibits a high degree of exfoliation, as indicated by arches, domes and layered rock sheets. **b**, Instrumentation set-up in the region indicated by the white box in **a**, to collect temperature, light intensity, humidity and crack aperture data (symbols). **c**, Results of repeat terrestrial lidar scanning (black equals no data) indicate an inward deformation pattern (blue colours) over 63% of the sheet between afternoon and morning, consistent with overnight cooling. Error bounds shown in the histogram (white colour) account for 25% of the data, with the remainder (12%, oranges intermixed with blue contraction pixels) attributed to laser attenuation and incident angle error (see Methods).

daylight hours (Fig. 2). However, we infer that temperature exerts the dominant role in driving deformation, as the sheet deforms synchronously with temperature even when light intensity is minimal (that is, on cloudy days). Similarly, we found comparatively little influence between absolute humidity (after correcting relative humidity for temperature effects) and sheet deformation.

The daily temperature–deformation response is hysteretic and bounded (that is, heating and cooling cycles follow different but parallel pathways through time). Daily cycles form hysteresis loops in which both rapid morning heating and rapid afternoon cooling result in little resultant deformation (Fig. 3). In late morning, outward deformation tracks linearly with increasing temperature until peak temperatures are reached in the afternoon. Following rapid afternoon cooling with little resultant deformation, more gradual cooling occurs coincident with linear inward deformation. On a seasonal cycle, cumulative outward deformation peaks during the warmest months (June through September) and is on average 21 mm greater than the maximum inward deformation that occurs during the coolest months (November through February; Fig. 4). This suggests that some rockfalls might be more likely during hot summer months, when exfoliation sheets are at their maximum outward position from cliffs. However, the maximum range of daily deformation does not coincide with the warmest times of the year, but rather with the greatest daily temperature range—typically in March–April and October–November. These periods may be times when rock damage at crack tips is most likely to occur.

Measurements of the maximum monthly outward movement of the sheet indicate that cumulative outward deformation occurred over 3.5 years (Fig. 4). This is coincident with a slight warming trend measured at both the exfoliation sheet (0.05 °C/month) and in greater Yosemite Valley (0.04°/month). At the lowest sensor, the sheet moved away from the cliff at nearly 1 mm yr^{-1}, whereas at the upper sensors the sheet moved outwards at half this rate. The bottom attachment points of vertically oriented exfoliation sheets are subjected to greater gravitational stresses than those above—thus accelerated crack opening should be expected at the bottom attachment due to the superimposed gravitational load. Fracture opening is known to be a nonlinear process[32]; as such, we cannot use our measured deformation rates to extrapolate back to when the exfoliation fracture might have formed, nor to predict

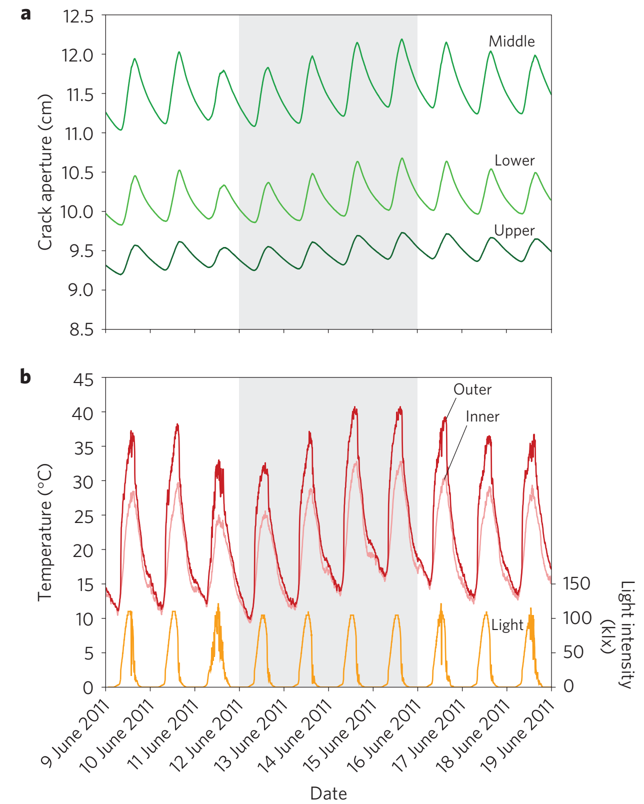

Figure 2 | Daily deformation and temperature data. a,b, Exfoliation sheet deformation (**a**) closely tracks both near-rock surface temperature and light intensity (**b**), a proxy for solar radiation. In **a**, upper, middle and lower labels represent the data from the three sensors ordered from top to bottom as shown in Fig. 1b. In **b**, data are from the middle sensors on the outside and inside of the sheet as shown in Fig. 1b. Overall crack aperture and daily deformation is larger at the middle of the sheet, coincident with the expected structural response of an end-supported beam deforming from thermal bowing and expansion. Shaded area delineates the aperture and temperature data shown in Fig. 3.

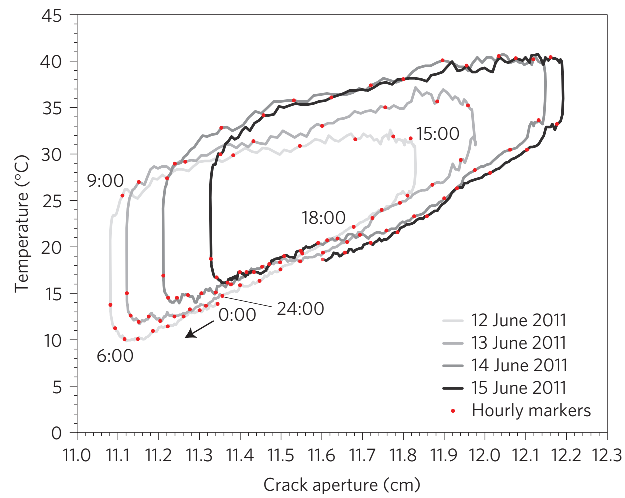

Figure 3 | Daily hysteresis loops of temperature–crack aperture (flake deformation) data. Loops maintain similar shape and size over time, but increase in overall magnitude with sequentially increasing daily temperatures. Labels at three-hour increments are shown only on the earliest loop, with the clockwise direction of all loops shown by an arrow starting at 0:00. Data for the middle crackmeter and middle outer temperature sensor are shown.

the future detachment of the sheet. However, research suggests that past fracturing in Yosemite Valley has occurred under slow (subcritical) conditions[14].

Thermodynamic framework

One-dimensional thermodynamic analysis comparing the energy needed to heat an exfoliation sheet versus the energy available from the environment shows that exfoliation sheets are easily capable of large temperature increases during diurnal warming. First, we calculate the amount of heat (Q) required to increase the temperature (ΔT) of an exfoliation sheet assuming typical[33] specific heat capacity (c) and mass (m) of the studied exfoliation sheet as determined from measured density properties for granodiorite and a computed volume of the sheet from lidar data (Supplementary Table 1):

$$Q = cm\Delta T \tag{1}$$

For a 20 °C temperature change (see Fig. 3) the energy required to heat the sheet is 3.1×10^5 kJ. Next, we assume that the source of heating is provided only by a thermal gradient across the sheet thickness, computed by subtracting the measured temperatures at the front and back of the sheet. This conservatively ignores the process of radiation, which is initially responsible for heating the outside of the sheet, but the analysis is simplified considerably if we focus only on heat transfer within the sheet; our calculation for the time required for heating is therefore a maximum estimate. The average maximum daily gradient (ΔT_g) across the sheet over 3.5 years was 13.3 °C (although it often exceeded 20 °C during winter months). Using Fourier's Law for conductive heat transfer[34]:

$$q = -k\Delta T_g A_s / d \tag{2}$$

a full sheet thickness (d) of 10 cm, a typical value[35] for thermal conductivity (k), and the sheet surface area (A_s) (Supplementary Table 1), we estimate the average heat input (q) to be 31 kJ s^{-1} to the rock sheet. Under these conditions, full-thickness heating of the sheet can increase the temperature by 20 °C in approximately 3 h. Alternative approaches to this analysis (for example, using thermal diffusivity to model heating across a cross-section of the sheet) provide similar results of the same order of magnitude. Our analysis results are nearly identical to the measured time required for initial, morning heating of the sheet (left side of cycles in Fig. 3) and matches measured time delays between heating and deformation in similar settings[28].

A thermodynamic Carnot cycle provides an analogy to the measured temperature-dependent deformation response, with thermodynamic process entropy replaced with crack aperture deformation. A thermally deforming exfoliation sheet can be thought of as a heat engine, with temperature cycles driving the oscillation of the sheet 'piston' outwards from, and inwards towards, the cliff (Fig. 3). Although our crack aperture data records real process cycles rather than idealized Carnot heat cycles, the analogy between isothermal processes with crack aperture opening and closing, and similarly for isentropic processes with crack aperture stability, provides a framework for understanding the system mechanics. Thermal energy is transformed to mechanical energy through the oscillation of exfoliation sheets outwards and inwards perpendicular to cliffs. The difference in the energy provided to a rock sheet during the opening phase and that delivered back to the environment during the closing phase is the work performed by the system—directly analogous to a Carnot cycle. Although our deflection measurements do not provide the information needed to perform a complete energy–work analysis within a thermodynamic

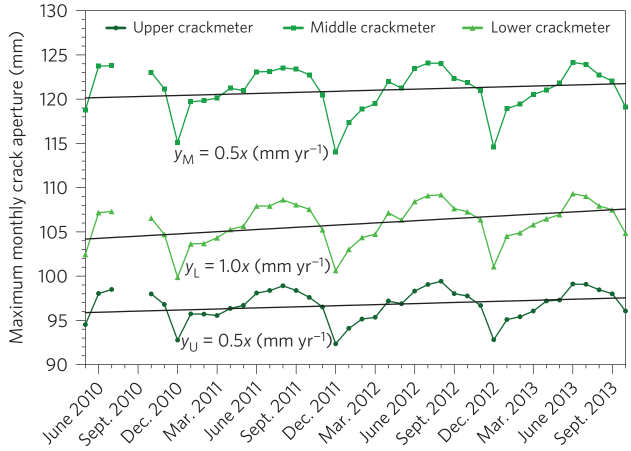

Figure 4 | Maximum monthly crack aperture time series data showing seasonal and annual deformation patterns. Long-term trends, based on three consecutive years of data (October 2010 to October 2013), show up to 1 mm yr^{-1} cumulative outward deformation. y_U, y_M and y_L represent the long-term maximum monthly crack aperture for the upper, middle and lower signals as a function of the length of time (x) in years. Data from August and September 2010 are incomplete.

framework, we propose, and show next through structural and fracture analysis, that energy absorbed by the system must lead not only to sheet deformation but also to rock fracture at the sheet endpoints.

Analysis of loads and deformations

Heating of exfoliation sheets can lead to two potential deformation effects: thermal bowing as a result of imposed thermal gradients across rock sheets, and thermal expansion as a result of uniform heating of entire sheets. The two are not mutually exclusive, and result from the particular temperature regime to which the rock is exposed. Research on the effects of fires on structural beams provides direct analogies to the effects of heating on partially detached rock sheets[36]. Thermal gradients across exfoliation sheets result in subsequent differential deformation, with expansion and tension on the hot (outer) side, and contraction and compression on the cooler (inner) side (Fig. 5). If a mechanism exists for the sheet ends to rotate outwards (that is, so-called 'pinned' connections provided, for example, by damaged zones at crack tips), outward deflection (thermal bowing) will occur with curvature ($\varphi = \alpha \Delta T_g / d$) induced by the thermal gradient and with subsequent thermal gradient longitudinal strains (ε_φ) in the exfoliation sheet[36]:

$$\varepsilon_\varphi = 1 - \frac{\sin(L\varphi/2)}{(L\varphi/2)} \quad (3)$$

For the monitored exfoliation sheet geometry (Supplementary Table 1), previously measured ΔT_g, and typical[37] coefficient of thermal expansion (α), ε_φ is 1.70×10^{-5}.

If the thermal regime is sufficient to cause full-thickness heating of the sheet, as shown to occur from our thermodynamics analysis, the resultant uniform temperature increase (ΔT) will lead to thermal expansion longitudinal strains (ε_{th}) throughout the sheet:

$$\varepsilon_{th} = \alpha \Delta T \quad (4)$$

For a 20 °C increase in temperature, ε_{th} is 1.60×10^{-4}. These two longitudinal strains, ε_φ and ε_{th}, work in the same direction at the exterior of the sheet and in opposite directions at the interior of the sheet, with ε_φ forcing the sheet exterior into tension and the sheet interior into compression, and ε_{th} forcing the entire sheet into tension (relative to their initial conditions; Fig. 5). Working the geometric problem related to the theoretical outward deflection of the exfoliation sheet (see Methods) indicates the measured daily deformation (~8.5 mm; for example, Fig. 3) is much less than that generated by thermal sources (23–31 mm). Outward deformation therefore accounts for only a portion of the potential thermal strain energy—the remainder must be manifest as additional stress at the sheet endpoints. When an exfoliation sheet is laterally restrained at the endpoints (but pinned and free to rotate open, Fig. 5), as is typical for many partially detached sheets, resultant thermal stresses (σ_{rt}) will develop and can be computed by elastic theory:

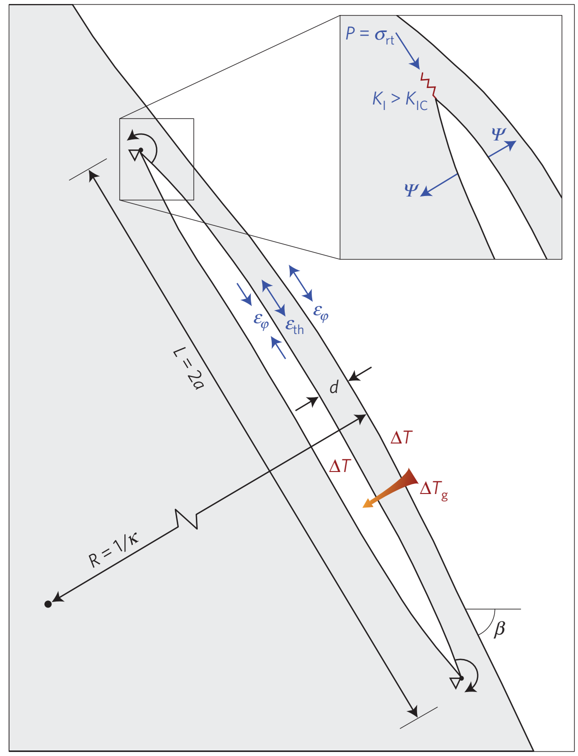

Figure 5 | Exfoliation sheet geometry and fracture model. The geometry is defined here by L, exfoliation sheet fracture length; d, exfoliation sheet thickness as measured perpendicular to the rock surface; κ, topographic curvature and β, topographic slope of the exfoliation sheet. Lateral restraint (that is, pinned connections shown by triangles indicating only rotation is allowed) at sheet endpoints leads to strains (and stresses) from uniform heating (ΔT; tension, ε_{th}) and thermal-gradient-induced bowing (ΔT_g; compression and tension, ε_φ). Resultant crack tip compressional stress ($P = \sigma_{rt}$, acting in opposite and equal reaction to tensile strains in the sheet) and subsequent orthogonal tensile stress (Ψ) lead to fracture at the crack tips via the opening (type 1) mode when K_I, the stress intensity factor for mode I opening, exceeds the material state parameter K_{IC}.

$$\sigma_{rt} = E(\varepsilon_{th} \pm \varepsilon_\varphi) \quad (5)$$

where E is the elastic modulus (Supplementary Table 1). Using our measured thermal conditions ($\Delta T = 20$ °C, $\Delta T_g = 13.3$ °C), the resultant thermal compressive stress at the crack tips is between 4,600 and 5,700 kPa. These represent maximum stresses resulting from thermal longitudinal strain. Are stresses of this magnitude capable of causing initial instability and subsequent fracture?

Fracture, crack propagation and rockfall

Recent work has shown that compressive stresses acting parallel to a curved surface generate tensile stresses normal to that surface[16,17,38]. For partially detached exfoliation sheets, this effect causes fractures behind sheets to be stressed in an opening (Mode I) mode[32] (Fig. 5). The tensile stress (Ψ) normal to the fracture opening direction is based on both a rock curvature stress term and a gravitational stress term[17,38]:

$$\Psi = (\kappa P - \rho g \cos \beta) d \tag{6}$$

where κ is the rock curvature (equal to the inverse of the radius of curvature (R) and negative where convex; Supplementary Table 1), P is the compressional stress perturbation (in this case, σ_{rt} and negative for compression), ρ is the rock density (Supplementary Table 1), g is the gravitational acceleration, β is the average rock surface slope (Supplementary Table 1), and d is the fracture depth below the surface (here, equal to the sheet thickness). For the monitored sheet, the thermally induced tensile stress acting to open the existing surface-parallel fracture is on the order of 2 to 4 kPa.

Tensile opening stresses on a fracture are typically analysed using the stress intensity approach from fracture mechanics[32]. The formula governing whether rock fracture will occur is given by:

$$K_{\mathrm{IC}} < K_{\mathrm{I}} = \Delta\sigma \sqrt{\pi a} \tag{7}$$

where K_{IC} is the Mode I (opening) fracture toughness (a state parameter that describes the ability of a material containing a crack to resist fracture), K_{I} is the stress intensity factor for mode I opening, $\Delta\sigma$ is the tensile stress perturbation (here equal to Ψ), and a is the half-length crack opening (taken as half of the total sheet detachment length for partially detached exfoliation sheets; Fig. 5). Exfoliation sheet crack tips may undergo mixed mode loading (that is, Mode I + Mode II (tearing)), but we evaluated only Mode I fracture for simplicity. Using values for the monitored sheet, we have K_{I} equal to between 0.01 and 0.02 $\mathrm{MPa}\sqrt{\mathrm{m}}$ (note that these units result from equation (7), where K_{I} is proportional to the square root of the crack half-length). Assuming a slightly larger value of α in the strain calculations, K_{I} may be an order of magnitude larger.

Do these thermally induced stress intensities exceed the fracture toughness? Measured K_{IC} values from detached boulders collected near the exfoliation sheet (Supplementary Table 1) are approximately 0.7 $\mathrm{MPa}\sqrt{\mathrm{m}}$ and back-calculated K_{IC} values from fracture propagation studies of Sierra Nevada granodiorite[39] reach as low as 0.04 $\mathrm{MPa}\sqrt{\mathrm{m}}$. Although the thermally induced stress intensity may be at the low end of the static fracture toughness of these rocks, we know that cyclic loading[23,31,40] and increasing temperature[41] can cause subcritical crack growth in rock when K_{I} exceeds K_0, the stress corrosion limit. Whereas a lower (stress corrosion) limit K_0 is unknown, existing data[42] suggest it may be 10% of K_{IC} (that is, ~0.004–0.07 $\mathrm{MPa}\sqrt{\mathrm{m}}$) and potentially lower[23]. Thus, with repeated diurnal cycles over tens to thousands of years, even stress intensities caused by heating may propagate existing sheeting fractures. We propose that this process not only progressively destabilizes exfoliation sheets but can also act as a rockfall trigger.

Implications of cyclic thermal deformation

We have demonstrated how cycles of heating and cooling lead to deformation, work cycles, and stresses capable of fracturing granitic exfoliation sheets. Our results have important implications for the triggering of rockfalls in exfoliating landscapes. First, our measurements indicate that seemingly static bedrock landscapes are, in fact, quite dynamic; that a 20 tonne sheet of rock can deform in and out of a near-vertical cliff face by up to 1 cm on a daily basis demonstrates the inherent instability of sheeted cliffs. Second, the observed cumulative outward deflection highlights a potential positive feedback loop in promoting detachment of exfoliation sheets. Namely, as crack opening occurs, sheet curvature increases, and likewise tensile stresses (equation (6)). These changes will, in turn, promote still higher values of stress intensity and lead to propagation of fracture tips. Further opening may occur as loose blocks become wedged at the bottom of fractures, preventing full return of sheets to their original position[43]. Both increasing temperature and temperature fluctuations may also promote fracture. Thus, we expect that rates of deformation should increase for already partially detached exfoliation sheets, albeit nonlinearly. Finally, our results offer a potential explanation for rockfalls that have no recognized trigger despite sometimes detailed observation at the time of failure. These include records of spontaneous summertime rockfalls in Japan[27], France[28], Brazil[31], Switzerland[44] and Yosemite[45]. In Yosemite[45], a disproportionate number (15%) of rockfalls with either an identified thermal stress trigger or an unrecognized trigger occur during the hottest summer months (July through September) and at the hottest times of the day (12:00 through 18:00 PST) compared to what would be expected under a random distribution (6%). We suggest that cyclic thermal stresses might be the trigger for these rockfalls and potentially many others around the world, highlighting the role of temperature in eroding steep landscapes.

Methods

Methods and any associated references are available in the online version of the paper.

Received 18 September 2015; accepted 24 February 2016; published online 28 March 2016

References

1. Hungr, O., Evans, S. & Hazzard, J. Magnitude and frequency of rockfalls and rock slides along the main transportation corridors of south-western British Columbia. *Can. Geotech. J.* **36,** 224–238 (1999).
2. Chau, K. T., Wong, R., Liu, J. & Lee, C. Rockfall hazard analysis for Hong Kong based on rockfall inventory. *Rock Mech. Rock Eng.* **36,** 383–408 (2003).
3. Rosser, N. J., Lim, M., Petley, D. N., Dunning, S. A. & Allison, R. J. Patterns of precursory rockfall prior to slope failure. *J. Geophys. Res.* **112,** F04014 (2007).
4. Oppikofer, T., Jaboyedoff, M. & Keusen, H.-R. Collapse at the eastern Eiger flank in the Swiss Alps. *Nature Geosci.* **1,** 531–535 (2008).
5. Ward, D. J., Anderson, R. S. & Haeussler, P. J. Scaling the Teflon peaks: rock type and the generation of extreme relief in the glaciated western Alaska Range. *J. Geophys. Res.* **117,** F01031 (2012).
6. Wieczorek, G. F. & Jäger, S. Triggering mechanisms and depositional rates of postglacial slope-movement processes in the Yosemite Valley, California. *Geomorphology* **15,** 17–31 (1996).
7. Krautblatter, M., Moser, M., Schrott, L., Wolf, J. & Morche, D. Significance of rockfall magnitude and carbonate dissolution for rock slope erosion and geomorphic work on Alpine limestone cliffs (Reintal, German Alps). *Geomorphology* **167–168,** 21–34 (2012).
8. Moore, J. R., Sanders, J. W., Dietrich, W. E. & Glaser, S. D. Influence of rock mass strength on the erosion rate of alpine cliffs. *Earth Surf. Process. Landf.* **34,** 1339–1352 (2009).
9. Gilbert, G. K. Domes and dome structures of the High Sierra. *Bull. Geol. Soc. Am.* **15,** 29–36 (1904).
10. Matthes, F. E. *Geologic History of the Yosemite Valley* (US Geological Survey Professional Paper 160, US Geological Survey, 1930).
11. Jahns, R. H. Sheet structure in granites: its origin and use as a measure of glacial erosion in New England. *J. Geol.* **51,** 71–98 (1943).
12. Twidale, C. R. On the origin of sheet jointing. *Rock Mech.* **5,** 163–187 (1973).
13. Holzhausen, G. R. Origin of sheet structure. 1. Morphology and boundary conditions. *Eng. Geol.* **27,** 225–278 (1989).
14. Bahat, D., Grossenbacher, K. & Karasaki, K. Mechanism of exfoliation joint formation in granitic rocks, Yosemite National Park. *J. Struct. Geol.* **21,** 85–96 (1999).
15. Ziegler, M., Loew, S. & Moore, J. R. Distribution and inferred age of exfoliation joints in the Aar Granite of the central Swiss Alps and relationship to Quaternary landscape evolution. *Geomorphology* **201,** 344–362 (2013).
16. Martel, S. J. Effect of topographic curvature on near-surface stresses and application to sheeting joints. *Geophys. Res. Lett.* **33,** L01308 (2006).
17. Martel, S. J. Mechanics of curved surfaces, with application to surface-parallel cracks. *Geophys. Res. Lett.* **38,** L20303 (2011).
18. Higgins, J. D. & Andrew, R. D. in *Rockfall Characterization and Control* (eds Turner, A. K. & Schuster, R. L.) (Transportation Research Board, 2012).
19. Blackwelder, E. The insolation hypothesis of rock weathering. *Am. J. Sci.* **26,** 97–113 (1933).

20. Griggs, D. T. The factor of fatigue in rock exfoliation. *Geology* **44,** 783–796 (1936).
21. Siegesmund, S., Ullemeyer, K., Weiss, T. & Tschegg, E. K. Physical weathering of marbles caused by anisotropic thermal expansion. *Int. J. Earth Sci.* **89,** 170–182 (2000).
22. Siegesmund, S., Mosch, S., Scheffzük, Ch. & Nikoayev, D. I. The bowing potential of granitic rocks: rock fabrics, thermal properties and residual strain. *Environ. Geol.* **55,** 1437–1448 (2008).
23. Chau, K. T. & Shao, J. F. Subcritical crack growth of edge and center cracks in façade rock panels subject to periodic surface temperature variations. *Int. J. Solids Struct.* **43,** 807–827 (2006).
24. McFadden, L. D., Eppes, M. C., Gillespie, A. R. & Hallet, B. Physical weathering in arid landscapes due to diurnal variation in the direction of solar heating. *GSA Bull.* **117,** 161–173 (2005).
25. Eppes, M. C., McFadden, L., Wegmann, K. & Scuderi, L. Cracks in desert pavement rocks: further insights into mechanical weathering by directional solar heating. *Geomorphology* **123,** 97–108 (2010).
26. Eppes, M. C., Willis, A., Molaro, J., Abernathy, S. & Zhou, B. Cracks in Martian boulders exhibit preferred orientations that point to solar-induced thermal stress. *Nature Commun.* **6,** 6712 (2015).
27. Ishikawa, M., Kurashige, Y. & Hirakawa, K. Analysis of crack movements observed in an alpine bedrock cliff. *Earth Surf. Process. Landf.* **29,** 883–891 (2004).
28. Gunzburger, Y., Merrien-Soukatchoff, V. & Guglielmi, Y. Influence of daily surface temperature fluctuations on rockslope stability: case study of the Rochers de Valabres slope (France). *Int. J. Rock Mech. Min. Sci.* **42,** 331–349 (2005).
29. Vlcko, J. *et al*. Rock displacement and thermal expansion study at historic heritage sites in Slovakia. *Environ. Geol.* **58,** 1727–1740 (2009).
30. Gischig, V. S., Moore, J. R., Evans, K. F., Amann, F. & Loew, S. Thermomechanical forcing of deep rock slope deformation: 1. Conceptual study of a simplified slope. *J. Geophys. Res.* **116,** F04010 (2011).
31. Vargas, E. A. Jr, Velloso, R. Q., Chávez, L. E., Gusmão, L. & Amaral, C. P. On the effect of thermally induced stresses in failures of some rock slopes in Rio de Janeiro, Brazil. *Rock Mech. Rock Eng.* **46,** 123–134 (2012).
32. Lawn, B. *Fracture of Brittle Solids* 2nd edn (Cambridge Univ. Press, 1993).
33. Tipler, P. *Physics for Scientists and Engineers* 4th edn (W. H. Freeman & Co., 1999).
34. Carslaw, H. S. & Jaeger, J. C. *Conduction of Heat in Solids* (Oxford Univ. Press, 1946).
35. Clark, S. P. Jr in *Handbook of Physical Constants* (ed. Clark, S. P. Jr) Geol. Soc. America Memoir 97, 459–482 (Geological Society of America, 1966).
36. Usmani, A. S., Rotter, J. M., Lamont, S., Sanad, A. M. & Gillie, M. Fundamental principles of structural behaviour under thermal effects. *Fire Safety J.* **36,** 721–744 (2001).
37. Skinner, B. J. in *Handbook of Physical Constants* (ed. Clark, S. P. Jr) Geol. Soc. America Memoir 97, 75–96 (Geological Society of America, 1966).
38. Stock, G. M., Martel, S. J., Collins, B. D. & Harp, E. Progressive failure of sheeted rock slopes: the 2009–2010 Rhombus Wall rock falls in Yosemite Valley, California, USA. *Earth Surf. Process. Landf.* **37,** 546–561 (2012).
39. Segall, P. & Pollard, D. D. Joint formation in granitic rock of the Sierra Nevada. *Geol. Soc. Am. Bull.* **94,** 563–575 (1983).
40. Celestino, T. B., Bortolucci, A. A. & Nobrega, C. A. Determination of rock fracture toughness under creep and fatigue. *Rock Mech. Proc. 35th US Symp.* 147–152 (Balkema, 1995).
41. Nasseri, M. H. B., Tatone, B. S. A., Grasselli, G. & Young, R. P. Fracture toughness and fracture roughness interrelationship in thermally treated Westerly granite. *Pure Appl. Geophys.* **166,** 801–822 (2009).
42. Atkinson, B. K. & Meredith, P. G. in *Fracture Mechanics of Rock* (ed. Atkinson, B. K.) 111–166 (Academic, 1987).
43. Bakun-Mazor, D., Hatzor, Y. H., Glaser, S. D. & Santamarina, J. C. Thermally vs. seismically induced block displacements in Masada rock slopes. *Int. J. Rock Mech. Min. Sci.* **61,** 196–211 (2013).
44. Hasler, A., Gruber, S. & Beutel, J. Kinematics of steep bedrock permafrost. *J. Geophys. Res.* **117,** F01016 (2012).
45. Stock, G. M. *et al*. *Historical Rock Falls in Yosemite National Park, California (1857–2011)* (US Geological Survey Data Series 746, 2013); http://pubs.usgs.gov/ds/746

Acknowledgements

This work was supported by the USGS Landslide Hazards Program and the US National Park Service, Yosemite National Park. We thank B. Murchey (USGS) for supporting the efforts to initiate this work. F. Sandrone, L. Gastaldo, B. Matasci and M. Jaboyedoff (École Polytechnique Fédérale de Lausanne, Laboratory for Rock Mechanics and the Université de Lausanne, Institute of Earth Sciences Terre, Lausanne, Switzerland) performed laboratory testing of rock samples for rock mechanics characterization. We appreciate discussions with R. S. Anderson, M. E. Reid, S. J. Martel and J. R. Moore, who provided helpful suggestions and encouragement throughout the project. Any use of trade, firm, or product names is for descriptive purposes only and does not imply endorsement by the US Government.

Author contributions

G.M.S. conceived the project. B.D.C. designed the experiment and processed the data. B.D.C. and G.M.S. jointly collected and interpreted the data. B.D.C. developed the analyses and wrote the paper with input from G.M.S.

Additional information

Supplementary information is available in the online version of the paper. Reprints and permissions information is available online at www.nature.com/reprints. Correspondence and requests for materials should be addressed to B.D.C.

Competing financial interests

The authors declare no competing financial interests.

Methods

Exfoliation sheet instrumentation. Our instrumented exfoliation sheet is located 11 m above the base of a nearly 500-m-tall south-facing cliff in Yosemite Valley, California, USA. The sheet is supported at only the top and bottom; the sides and middle are entirely detached from the cliff, forming a symmetrically tapering open fracture with 12 cm maximum aperture behind the sheet (Fig. 1b). The sheet terminates directly into the main rock mass at the bottom, with no indication of a bounding fracture (that is, full attachment). At the top, it terminates at a closed regional joint (that is, probable partial detachment), which restrains sheet deformation. Geomorphologically, this exfoliation sheet typifies those found throughout Yosemite and other granitic landscapes worldwide. We installed three strain gauges between the back of the sheet and the underlying cliff face (Fig. 1b) and measured absolute deformation at 5-min intervals from May 2010 through October 2013. We coupled these data with simultaneous records of near-rock-surface air temperatures and relative humidity on the inner and outer sheet surfaces, and light intensity (illuminance) on the outer sheet surface.

We measured changes in crack aperture using modified Geokon Model 4420 crackmeters with scissor-jack-type, 5.1 cm by 7.6 cm rectangular platens epoxied between the stable cliff and deforming sheet. The crackmeters record changes in vibrating wire strain frequencies, which we transformed to relative fracture deformation distance using laboratory-based polynomial calibrations of the frequency signal. Manufacturer specifications for resolution and accuracy are 0.0125 mm and 0.05 mm respectively. Crackmeters were located 30 cm inwards from the more open (that is, 10–12 cm wide) edge of the sheet, at the quarter, half and three-quarter points along the sheet length. Signal noise was removed by comparing data with those from an additional control crackmeter with fixed 12.1 cm aperture placed perpendicularly behind (but not affixed to) the midpoint of the sheet near the middle crackmeter. Control crackmeter signal noise (0.4 mm) was well below the typical average measured daily response (5–10 mm) from the other crackmeters, with the exception of six discrete events when the control crackmeter jammed between the cliff and sheet. The jams were due to rotation of the control unit during periods of extreme contraction of the sheet. We fixed the rotational issue in December 2012 following the last jamming event. For the six events, each lasting between 3 and 8 days (in MM/DD-DD/YYYY format: 11/19-21/2010, 05/07-10/2011, 10/09-12/2012, 10/22-24/2012, 11/08-10/2012, 12/12-19/2012), the control data was corrected by adding the difference in control readings before and after the jam by using the average of three stable days of similar temperature before and after the jamming event.

We measured near-rock-surface (that is, 2 cm from the rock surface) air temperature (as a proxy for surface rock temperature) and surface light intensity (averaging wavelength response between 200 and 1,200 nm) using Onset Hobo pendant-type data loggers mounted on the outer and inner sheet surfaces and that were time-synchronized with the crackmeters. We analysed long-term temperature trends over the experiment period by using our pendent data sets along with temperature data from the weather station at Yosemite National Park Headquarters (station #049855; http://www.wrcc.dri.edu/cgi-bin/cliMAIN.pl?ca9855), located 1.6 km east of the study site.

Terrestrial lidar deformation monitoring. We confirmed the deformation pattern through stationary, repeat terrestrial lidar scans collected three times over an 18-h period using a Riegl Z420i laser scanner at 30 m range. The data have 1.5 cm mean point spacing with calculated ±1.2 mm change detection accuracy based on a best fit of seven non-coplanar control points located on stable (non-exfoliation sheet) areas both on and off the cliff. Our error estimate does not account for noise in the laser signal itself (that is, beam attenuation and non-oblique reflective incidence angle), which we estimate to be on the order of 3 to 10 mm, on the basis of an independent manufacturer calibration test performed on our scanner following data collection. This is consistent with others whom have performed similar close-range (<50 m) lidar calibration studies[46]. Despite the absolute error of our data being greater than 1.2 mm (as shown by the histogram tails with unlikely large displacements in Fig. 1c), we present the full histogram outside this range to ensure that the local deformation signal throughout the exfoliation sheet is not masked by the error bars. The lidar-derived deformations ranged between 0.8 mm and 1.9 mm of those measured by the crackmeters (that is, relative errors of between 13% and 44% of the crackmeter measurements) and captured the overall expected contractive deformation pattern of the exfoliation sheet during this time span. We also used the lidar data to determine the exact sheet geometry, including surface slope and curvature required for the fracture analyses.

Exfoliation sheet geometrical deformation analyses. We calculated the theoretical outward deformation of the exfoliation sheet by trigonometric considerations of the sheet geometry. Taking the undeformed sheet radius, $R_1 = 116.3$ m $(1/\kappa)$, and a known chord length, $L = 19$ m, the sagitta (the perpendicular distance between a chord and the outer circular segment), H is determined via Pythagorean Theorem to be 0.389 m. Circular arc geometry is then used to calculate the arc angle (θ_1), and consequently the undeformed arc segment length, $S_1 = 19.021$ m. The deformed arc length (S_2) is calculated by direct computation of the thermal expansion and bowing strains (ε_{th} and ε_φ) by multiplying S_1 by the quantity $[1+(\varepsilon_{th} \pm \varepsilon_\varphi)]$. This results in $S_2 = 19.024$ m. For simplicity, we assume that the sheet retains a circular shape when deformed outwards. This requires recomputation of the sheet geometry (both the new arc angle and radius) based on the new arc length (S_2) and fixed chord length ($L = 19$ m). An analytical expression can be solved iteratively that relates the arc angle (θ_2) to S_2 and L:

$$\sin(\theta_2/2) - L\theta_2/2S_2 = 0 \tag{8}$$

Solving for θ_2 and then R_2 (109.9 m and 107.6 m, respectively, for the minimum and maximum values of S_2 based on the range of computed strains), the sagitta of the deformed arc segment ($H + \Delta H$) is calculated (0.412–0.420 m) by trigonometric relations $[H + \Delta H = R2(1 - \cos(\theta_2/2))]$. The theoretical outward deformation of the flake ($\Delta H = 22.9$–31.4 mm) is then computed by subtracting the undeformed sagitta (H) from the deformed sagitta ($H + \Delta H$).

Rock mechanics material testing. Rock density (ρ), stiffness (E), and fracture toughness (K_{IC}) parameters for Half Dome Granodiorite were determined from laboratory testing conducted at École Polytechnique Fédérale de Lausanne Laboratory for Rock Mechanics (EPFL-LMR) in Lausanne, Switzerland. Boulder-sized (~ 0.03 m^3) samples were collected, cored, and tested under uniaxial compression (Swiss Standard SN 670 353) using cylindrical samples, and fracture toughness (International Society for Rock Mechanics, ISRM 1995 Standard Method for Determining Mode I Fracture Toughness) using cracked chevron notched Brazilian disc (CCNBD) samples.

Data sources. Crackmeter deformation, temperature, and light intensity data are available for the period of study beginning May 2010 through October 2013 in a Microsoft Excel file as part of the Supplementary Information. Two data sheets are available, one each for the crackmeter (sheet name: Crackmeter Data) and light and intensity data (sheet name: Temperature and Light Data). Metadata are included for each data set in the first fifteen lines of data. Long-term temperature data used in our analysis is available publicly at http://www.wrcc.dri.edu/cgi-bin/cliMAIN.pl?ca9855.

References

46. Abellán, A., Jaboyedoff, M., Oppikofer, T. & Vilaplana, J. M. Detection of millimetric deformation using a terrestrial laser scanner: experiment and application to a rockfall event. *Nat. Hazards Earth Syst. Sci.* **9,** 365–372 (2009).